ELSEVIER

Precambrian Research 79 (1996) 171–194

Precambrian Research

Geochemical and mineralogic effects of contact metamorphism on banded iron-formation: an example from the Transvaal Basin, South Africa

Alan J. Kaufman

Harvard University, Department of Earth and Planetary Sciences, 20 Oxford Street, Cambridge, MA 02138, USA

Received 1 January 1994; revised version accepted 1 December 1995

Abstract

Intrusion of a diabase sill into the Paleoproterozoic Kuruman Iron Formation, Transvaal Basin, South Africa makes it possible to distinguish between effects of contact and regional metamorphism on mineralogic, elemental and isotopic compositions of banded iron-formation (BIF) lithofacies. Temperatures within the aureole of contact metamorphism likely did not significantly exceed 450°C as suggested by the presence of early diagenetic carbonates, greenalite, and stilpnomelane (formed prior to intrusion) in chert-rich facies as close as 4 m from the sill. In sediments 32 m away from the intrusion, a temperature of ~280°C is indicated by the magnitude of ^{18}O fractionation between successive chert and siderite microbands; in unmetamorphosed equivalents similar isotopic analyses on whole-rock samples yield temperature estimates between 150 and 230°C.

In comparison with samples of similar lithofacies from the underlying Campbellrand–Kuruman transition zone, carbonates from within the metamorphic aureole are depleted in ^{13}C and ^{18}O. The abundance and C-isotopic composition of total organic C (TOC) in whole-rock samples is lower and more enriched in ^{13}C than those in samples outside of the zone of contact metamorphism. Within 5 m of the diabase sill the abundance of Fe increases dramatically and the oxidation state of the sediments fluctuates considerably more than in sediments outside of the metamorphic aureole. Isotopic and mineralogic systematics in the zone of contact metamorphism in the Kuruman Iron Formation are similar to those in siliceous dolomites and limestones altered by similar thermal processes. As the most distinct isotopic and elemental variations occur within 10 m of the diabase sill, it is suggested that volatilization and fluid infiltration associated with the intrusion were the main processes of alteration.

Consideration of the effects of metamorphism (both contact and regional) as well as early diagenesis on the mineralogy and isotopic chemistry of BIF sediments may be a key to our understanding of primary mineralogies and oxidation state of these enigmatic deposits.

1. Introduction

In the Paleoproterozoic Transvaal Basin of South Africa, the intrusion of a 5 m thick diabase sill into the Groenwater Member of the Kuruman Iron Formation resulted in the alteration of both the bulk mineralogy and the C- and O-isotopic composition of carbonates and organic C in banded iron-formation (BIF) lithofacies. These chemical sediments are especially well-suited for studies of contact meta-

SSDI 0301-9268(95)00093-3

morphism because they are otherwise structurally undeformed and of very low regional metamorphic grade (Klein and Beukes, 1989). Mineralogic evidence suggests that maximum regional diagenetic temperatures are on the order of 110–170°C at pressures of 2 kbar or less (Miyano and Beukes, 1984). In contrast, a temperature range of 150–230°C for unmetamorphosed BIFs has been calculated from the magnitude of ^{18}O fractionation between chert and siderite in whole-rock samples (Perry and Ahmad, 1983). For comparison, units unaffected by contact metamorphism within the transition from carbonate to BIF deposition have already been studied for systematic variations in mineralogy and elemental and isotopic compositions (Klein and Beukes, 1989; Beukes et al., 1990).

Because the patterns of mineralogic and isotopic variations in the metamorphic aureole broadly resemble those of regional metamorphic and early diagenetic processes (albeit localized and on a much shorter time scale), study of BIF sediments affected by contact metamorphism may yield important general information on the direction and magnitude of alteration in BIFs. As all BIFs are altered to some degree, a better understanding of diagenetic pathways should allow for a better estimate of primary mineralogies, isotopic compositions, and oxidation states. Such an analysis could be particularly important for evaluating elemental Fe concentrations of 'paleosol' samples from the Kuruman Iron Formation; Holland and Beukes (1990) concluded that nearly all original Fe^{2+} was oxidized and retained as Fe^{3+} in a BIF paleosol which may have resulted from a dramatic rise in atmospheric O_2 levels between 2.2 and 1.9 Ga ago.

In this study, isotopic compositions of total organic C (TOC) and of carbonate in mm-scale microbands, cm-scale mesobands, and whole-rock samples within the metamorphic aureole of the diabase sill are compared with similar samples unaffected by contact metamorphism. Temperatures within the metamorphic aureole are estimated from observed mineral assemblages, metamorphic reactions, and from the magnitude of O-isotopic contrast between successive chert and carbonate microbands. Further, results of this study are compared with those from studies of siliceous dolomites altered by contact metamorphism where systematic isotopic variations are attributed to the degree of volatilization, patterns of fluid circulation, and P–T–X conditions (Valley, 1986).

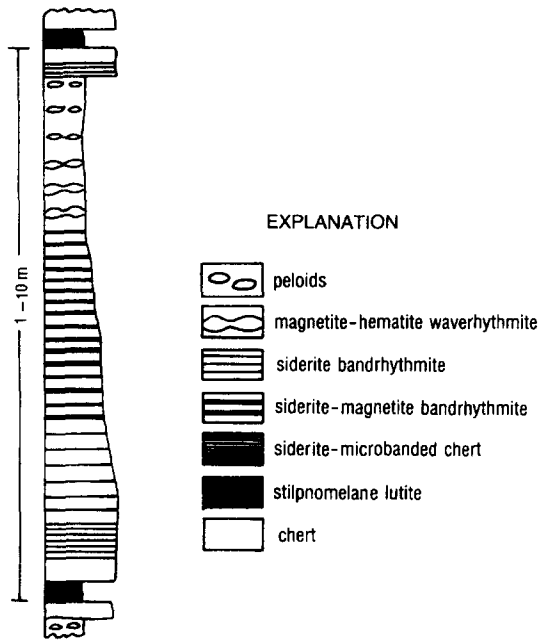

Fig. 1. Idealized example of a complete stilpnomelane lutite ferhythmite macrocycle (after Beukes, 1984).

2. Stratigraphy

A maximum age for the Kuruman Iron Formation is constrained by a volcanic ash bed near the contact with the underlying Campbellrand Subgroup which

Notes to Table 1:

[a] Mineral abbreviations: QTZ = chert, SID = siderite, ANK = ankerite, DOL = dolomite, GRN = greenalite, STL = stilpnomelane, MIN = minnesotaite, MAG = magnetite, HEM = hematite, PYR = pyrite.

[b] Mineral is designated as minor if it constitutes less than 5% of the sample.

[c] Diabase sill spans from 87.5 to 92.5 m in the Pomfret AD-5 core.

Table 1
Occurrence of BIF minerals in samples from the Groenwater Member of the Kuruman Iron Formation, South Africa [a,b]

sample (m)[c]	QTZ	SID	ANK	DOL	GRN	STL	MIN	MAG	HEM	PYR
79.94	x	minor	x		minor	x	x	x		
80.25	x	x				x	x	x		
80.30	x	x	minor			x	x	x		
80.50	x	x	minor			x		x		
80.70	x	x				x	x	x		
81.70	x	x	x		minor	minor	x	x		
81.85	x		x		minor	x	x	x		
82.00	x	x	minor		minor	x	x	x		
82.35	x		x		minor	minor	x	x		
82.58	x	x			minor	minor	x	x		
82.90	x					minor	minor	x		minor
83.05	x		x		minor	x	x	x		minor
83.40						x				minor
85.18						x		x		
85.55	x						x			
85.90	x	minor				x	x	x		
92.95	x			(x)		x	x	x		
93.22	x						x	x		
93.40	x			x				x		
93.75	x			x		x	x	x		
94.12	x						x			
94.40	x					x	x	x		
95.25	x						x	x		
95.72	x				x	x	x	x		
95.98	x		minor				x	x		
96.11	x		x				x			
96.25	x	minor	minor		minor		x	x		
96.40	x	minor	minor				x	x		minor
96.53	x	x	minor		minor		x	x		minor
96.89	x	x	x			x	x	x		minor
97.26	x		x		minor	x	x			
97.44	x					x	minor			
97.65	x	x				x	x	x		
98.35	x	x					x	x		
101.00	x	minor	minor			x	minor	minor		
101.36	x	x	x			x	x			
101.42	x		x				x	x		
101.77	x		x			minor	x	minor		
112.02	x		minor				x			
112.40	x						x	x		
112.88	x	minor	minor				x	x		
113.22	x	x	minor				x	x		
113.73	x	minor	x				minor			
114.23	x	x	x				x			
114.56	x	minor	x			x	x			
125.80	x	x	x			x	x			
132.84	x	x	x		minor		minor	x	x	minor
133.15	x	x	x				x	x		
134.41	x	x	x				minor	x	x	minor
135.60	x	x	x				minor	x	x	
136.55	x	x	x				minor	x		
136.78	x	minor	x		minor		x	x	x	
136.90	x	x	x				x		x	
140.93	x	x	x			x	minor		x	minor
141.10	x	x	x			x	minor	x	x	
141.62	x		minor				minor	x	x	
142.75	x	x	minor				x	x	x	
143.90	x	x				x	x	x	x	
144.04	x	x	x		minor		x	x	x	minor
144.12	x	x	x				x			

was dated by zircon U–Pb techniques to be 2521 ± 3 Ma (Sumner and Bowring, 1996). The Groenwater Member of the Kuruman Iron Formation is composed of stacked stilpnomelane lutite ferhythmite macrocycles (Fig. 1) which correspond to the alternation of S- and BIF-macrobands in the Dales Gorge Member of the Brockman Iron Formation (Trendall and Blockley, 1970; Beukes, 1980, 1983, 1984, 1987). Deposition of these cycles is thought to have been controlled by a combination of volcanic and biologic interactions (Beukes, 1983, 1984). A complete macrocycle consists, from the base upwards, of (1) stilpnomelane lutite, (2) siderite-microbanded chert, (3) siderite–magnetite band rhythmite, (4) magnetite–hematite ribbon rhythmite, and (5) siderite-microbanded chert. Individual cycles are 1 to 10 m thick, and five distinct macrocycles are present. Stilpnomelane lutite beds, interpreted as volcanic ash-fall deposits (LaBerge, 1966), often exhibit basin-wide lateral continuity, and are thus used as marker horizons. The abundance of chert in whole-rock samples and the thickness of chert mesobands gradually decrease upsection, and then increase sharply immediately below the next stilpnomelane lutite horizon (Beukes, 1980, 1984).

3. Materials and methods

3.1. Sample selection and preparation

Specimens from four sedimentary cycles in a 64 m interval of the Pomfret AD-5 diamond drill core were collected by N. Beukes (in 1986) and the author (in 1990). This core includes the transition from Campbellrand carbonates into the overlying Kuruman Iron Formation. Other specimens used in this study were collected by C. Klein and N. Beukes from well-correlated diamond drill cores at Whitebank (WB-98) and Coretsi (CN-109; see Fig. 1 of Klein and Beukes, 1989 for localities). A suite of 46 whole-rock samples representing all lithologies in the Pomfret core was used to determine variations in the C- and O-isotopic compositions of carbonates, and the abundance and C-isotopic composition of TOC. Seven samples were chosen for detailed analyses of mesobanded carbonates. Microbanded carbonates were analyzed in three samples from the AD-5 core and in two additional samples, one each from the WB-98 and CN-109 cores. Microbanded cherts were also analyzed for O-isotopic compositions in one of the AD-5 samples. Geochemical methods and

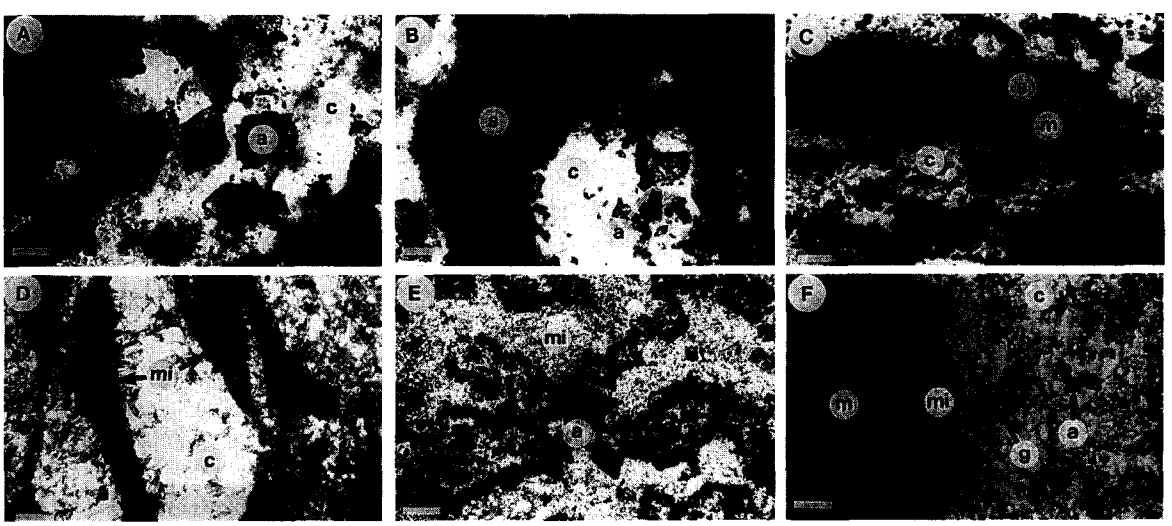

Fig. 2. Photomicrographs of Kuruman Iron Formation BIF samples. (A) Coarse-grained secondary ankerite (*a*) in a matrix of chert (*c*; sample 132.84A). (B) Siderite (*s*) microbands in chert matrix (sample 113.22). (C) Siderite microbands partially replaced by magnetite (*m*; sample 132.84B). (D) Siderite microbands replaced by minnesotaite (*mi*; sample 96.89). (E) Outlines of pre-existing ankerite rhombs in matrix of minnesotaite (sample 132.84). (F) Greenalite (*g*) coexisting with minnesotaite, siderite, ankerite, and chert (sample 144.04). Siderite grains appear dark due to staining procedure. Scale bar = 0.1 mm

fractionation factors employed in this study are discussed in detail by Kaufman et al. (1990).

4. Results and discussion

4.1. Petrographic analysis

Sixty thin sections from the Groenwater Member of the Kuruman Iron Formation were examined—the mineralogy of each is shown in Table 1. Lithologic variations are dependent on both the lithofacies and the effects of contact metamorphism. In this study, the mineralogic associations and the relative abundance of both iron-carbonates and -silicates are used to infer the extent of alteration caused by contact metamorphism.

The diabase sill extends from about 87.5 to 92.5 m in the Pomfret AD-5 drillhole. It is composed of randomly oriented, coarse-grained laths of plagioclase and euhedral coarse-grained olivine with an ophitic to subophitic texture. In a sample near the lower contact with BIF sediments (92.4 m) the diabase is composed of finer-grained plagioclase and the abundance of olivine is greater (this is likely due to the gravitational concentration of early formed olivine grains).

In BIF lithofacies, mineral assemblages consist of chert, siderite, members of the dolomite–ankerite series, magnetite, hematite, and minnesotaite with minor amounts of greenalite, stilpnomelane, pyrite, and riebeckite. These occur in mesobands, microbands, or as fine-grained inclusions in a chert- or magnetite-rich matrix. Fine-grained chert is the major constituent in all but a few magnetite- and hematite-rich samples (Table 1). Siderite is typically fine-grained (10–20 μm), granular to subhedral, and stains brown with Alizarin red S and 17 wt% NaOH. Ankerite and ferroan dolomite are medium- to coarse-grained (30–100 μm), euhedral, and are purple and light brown to beige after staining (Fig. 2A). Carbonate-rich mesobands are composed of siderite microsparite or coarse-grained ankerite. The matrix is either chert-rich, with minor iron silicates or iron oxides, or oxide-rich, with minor iron silicates and chert. Pure carbonate mesobands are present in some samples. In chert-rich facies, siderite is generally the predominant carbonate mineral; in oxide-rich facies, ferroan dolomite and ankerite predominate.

Carbonate microbands are typically composed of siderite in thin, often discontinuous laminae in a chert matrix (Fig. 2B). Siderite is also disseminated randomly throughout the chert. Where siderite microbands are partially or completely replaced by ankerite, laminations are generally thicker and discontinuous. Ankerite rhombohedra and nodules also occur in chert matrix not associated with carbonate laminations; these may be replacing disseminated siderite or chert (cf. Klein and Beukes, 1989). Petrographic and isotopic studies of microbanded carbonates in the Dales Gorge Member BIF, Western Australia suggest that dissolution of primary siderite and subsequent precipitation of coarse, rhombohedral ankerite likely occurred in zones permeable to oxidizing diagenetic solutions (Kaufman et al., 1990). These findings are consistent with the observation that ankerite is often concentrated along the interface between massive (and apparently impermeable) siderite micrite and chert mesobands. Replacement of siderite by ankerite requires a source of additional Ca^{2+} and Mg^{2+} which most likely accompanied diagenetic waters as suggested in the following reaction:

$$2FeCO_3 + Ca^{2+} + xMg^{2+} \rightarrow Ca[xMg(1-x)Fe](CO_3)_2 + xFe^{2+} \quad (1)$$

The euhedral character of the coarse ankerites suggests that grains formed early, prior to lithification (Klein and Beukes, 1989; Beukes et al., 1990; Kaufman et al., 1990; Winter and Knauth, 1992).

Siderite in these sediments is often replaced (either partially or completely) by medium- to coarse-grained magnetite (Fig. 2C). Magnetite is also observed to cut across pre-existing ferroan dolomite and ankerite. Alternatively, it has been suggested that fine- to medium-grained magnetite preserved as cryptalgal laminations in thick mesobands may also represent a primary precipitate (Klein and Bricker, 1977). Replacement of carbonate by magnetite may be diagenetic and/or metamorphic in origin. In unmetamorphosed sediments from the Dales Gorge BIF, magnetite apparently replaced siderite during diagenesis under conditions of low to intermediate O_2 (Kaufman et al., 1990). Within the aureole of contact

metamorphism, magnetite may have formed by metamorphic processes, perhaps by oxidation of siderite in the presence of hematite as shown below:

$$FeCO_3 + Fe_2O_3 \rightarrow Fe_3O_4 + CO_2 \quad (2)$$

Experimental results (French, 1971) indicate that this reaction occurs at ~370°C at pressures of 2 kbar, and these results are consistent with the thermodynamic stability of siderite in the presence of hematite (Robie et al., 1984). In contrast, thermodynamic calculations by Miyano (1987) suggest that reaction (2) occurs at 220 to 280°C at pressures of 1 to 2 kbar (depending on $X(CO_2)$ in fluids and X_{Fe}^{sid}). However, unless Fe_2O_3 is present in contact, or at least in the immediate vicinity of the siderite, it is more likely that magnetite formed by decomposition of siderite as suggested by the reaction:

$$3FeCO_3 + H_2O \rightarrow Fe_3O_4 + 3CO_2 + H_2 \quad (3)$$

At 2 kbar, this reaction has been shown to occur at ~450°C (French, 1971). This temperature likely represents the upper stability limit for iron carbonates in the Kuruman Iron Formation.

The overall abundance of carbonate minerals in BIF facies generally decreases towards the diabase sill, although both early diagenetic ankerite and siderite persist as minor or trace constituents in chert-rich BIF lithofacies as close as 4 m (Table 1). In carbonate lithofacies intercalated with BIF lithofacies (samples from 93.40 and 93.75 m) Fe-rich dolomites are very coarse-grained and highly twinned apparently due to the effects of contact metamorphism. These samples also contain cryptalgal laminations of magnetite (which are highly convoluted) but no chert or other iron-silicates. A single sample of magnetite-rich stilpnomelane lutite immediately below the diabase (92.95 m) also contains abundant coarse-grained Fe-rich dolomite. The abundance and poikilotopic texture of the dolomite in this sample suggests, however, that its formation post-dated the intrusion. The decrease in abundance of ankerite and siderite in chert-rich BIF lithofacies near the diabase sill is likely due to effects of volatilization, escape of fluids (commonly CO_2 and H_2O), and/or formation of metamorphic minerals (Valley, 1986). Nonetheless, the presence of residual siderite and ankerite in samples adjacent to the heat source suggests that temperatures did not significantly exceed 450°C (French, 1971; Robie et al., 1984; Miyano and Klein, 1986).

Minnesotaite also forms under metamorphic conditions at the expense of greenalite, stilpnomelane, or iron carbonates and chert (French, 1973; Klein, 1974; Gole, 1980; Haase, 1982; Miyano, 1987). It is intimately intermixed with chert in all occurrences. In the Groenwater Member, Klein and Beukes (1989) and Beukes et al. (1990) suggest that minnesotaite in oxide-rich BIF forms by high temperature ($T \geqslant 250$°C depending on $X(CO_2)$; Miyano, 1987) reaction of siderite and quartz as shown in the following reaction:

$$3FeCO_3 + 4SiO_2 + H_2O \rightarrow Fe_3Si_4O_{10}(OH)_2 + 3CO_2 \quad (4)$$

These authors also show that the abundance of minnesotaite increases towards the diabase sill. In numerous samples close to the diabase sill, laminae which were likely composed initially of siderite are now completely replaced by minnesotaite (Fig. 2D). The formation of minnesotaite by reaction of siderite and chert requires a source of water; thus, variations in the abundance of minnesotaite may be linked to variations in the permeability of BIF sediments. Fluid infiltration rates can be enhanced in sediments affected by contact metamorphism (Valley, 1986). Zones where both ankerite and minnesotaite coexist were more likely more permeable to fluids which mediated (1) the alteration of siderite to ankerite during diagenesis and (2) the formation of minnesotaite from siderite and chert during contact metamorphism.

Further from the sill, petrographic observations indicate that formation of minnesotaite may not be controlled solely by reaction (4). Increase in the abundance of minnesotaite does not correlate with a decrease in the abundance of siderite. In fact, in minnesotaite-rich cherts, rhombohedral ankerite and ferroan dolomite are typically corroded or almost completely replaced by minnesotaite while coexisting siderite appears unaffected. Often only outlines of pre-existing ankerite rhombohedra remain (Fig. 2E). In these samples, minnesotaite likely forms at the expense of greenalite through dehydration during

low temperature ($100 \leqslant T \leqslant 150°C$ depending on X_{Fe}^{grn}) reaction with chert:

$$Fe_3Si_2O_5(OH)_4 + 2SiO_2 \rightarrow Fe_3Si_4O_{10}(OH)_2 + H_2O \quad (5)$$

Water released during reaction (5) may have contributed to the partial dissolution or 'corrosion' of ankerite rhombohedra.

In unmetamorphosed equivalents, Beukes (1980) indicates that the abundance of greenalite increases from the base to the top of the Groenwater Member. Within the zone of contact metamorphism it occurs as a minor constituent *always* coexisting with magnetite and stilpnomelane, only occasionally with siderite, ankerite, minnesotaite and chert (Table 1; Fig. 2F). Due to its general presence as a remnant mineral in fine-grained mixtures of magnetite and stilpnomelane (greater abundances of organic C are also noted in these assemblages), it appears that greenalite was preserved within the metamorphic aureole when the oxidation state of the local environment was buffered by an assemblage of reduced minerals and organic C, most importantly magnetite. Additional control on the oxidation states of BIF sediments may be exerted by variations in the permeability of the different lithofacies—with chert-rich facies being most open to the exchange of fluids (cf. Kaufman et al., 1990).

Combined with earlier isotopic arguments (Kaufman et al., 1990), these petrographic observations suggest that the BIF sediments were variably permeable to external fluids, thereby allowing for variations in the degree of alteration of lithofacies (for a contrasting view see Gregory and Criss, 1986).

Finally, while the abundance of the iron-silicate stilpnomelane appears to generally decrease approaching the sill (likely due to replacement by minnesotaite), it persists in several samples immediately adjacent to the diabase. Miyano and Klein (1989) present petrologic data that corroborates both experimental and theoretical estimates suggesting that the upper stability limit of stilpnomelane in iron-formation ranges between 430 and 470°C and 5–6 kbar. The persistence of this mineral (like iron-carbonates)

Table 2
Oxygen-isotopic composition of successive chert and carbonate microbands from a sample at 125.8 m depth in Pomfret AD-5 core, Kuruman Iron Formation, South Africa [a]

Vertical distance[b] (mm)	mineralogy[c]	δ_o(PDB)	δ_o(SMOW)	Δ(QTZ-SID)[c,d]
		(‰)		
3.5	SID	-9.75	20.81	
4.2	QTZ	-8.40	22.20	1.39, 0.92
5.0	SID	-9.29	21.28	
5.5	QTZ	-8.42	22.18	0.90, 0.85
6.0	SID	-9.25	21.33	
6.7	QTZ	-8.49	22.11	0.78, 1.15
7.5	SID	-9.60	20.96	
8.3	QTZ	-8.39	22.21	1.25, 1.05
9.0	SID	-9.41	21.16	
9.5	QTZ	-8.49	22.11	0.95, 1.16
10.0	SID	-9.61	20.95	

[a] Reported values represent means of duplicate measures. Uncertainties calculated as 95% confidence limits for δ_o (QTZ) and for δ_o (SID) are 0.27‰ and 0.34‰, respectively.
[b] Vertical distance measurement on polished core segment relative to arbitrary zero point at center of first carbonate microband analyzed in each segment (see Table 3).
[c] Mineralogy determined by petrographic analysis: QTZ = quartz, SID = siderite (contains minor amounts of coarse-grained ankerite).
[d] Isotopic difference calculated between chert microband and siderite microbands immediately above and below.

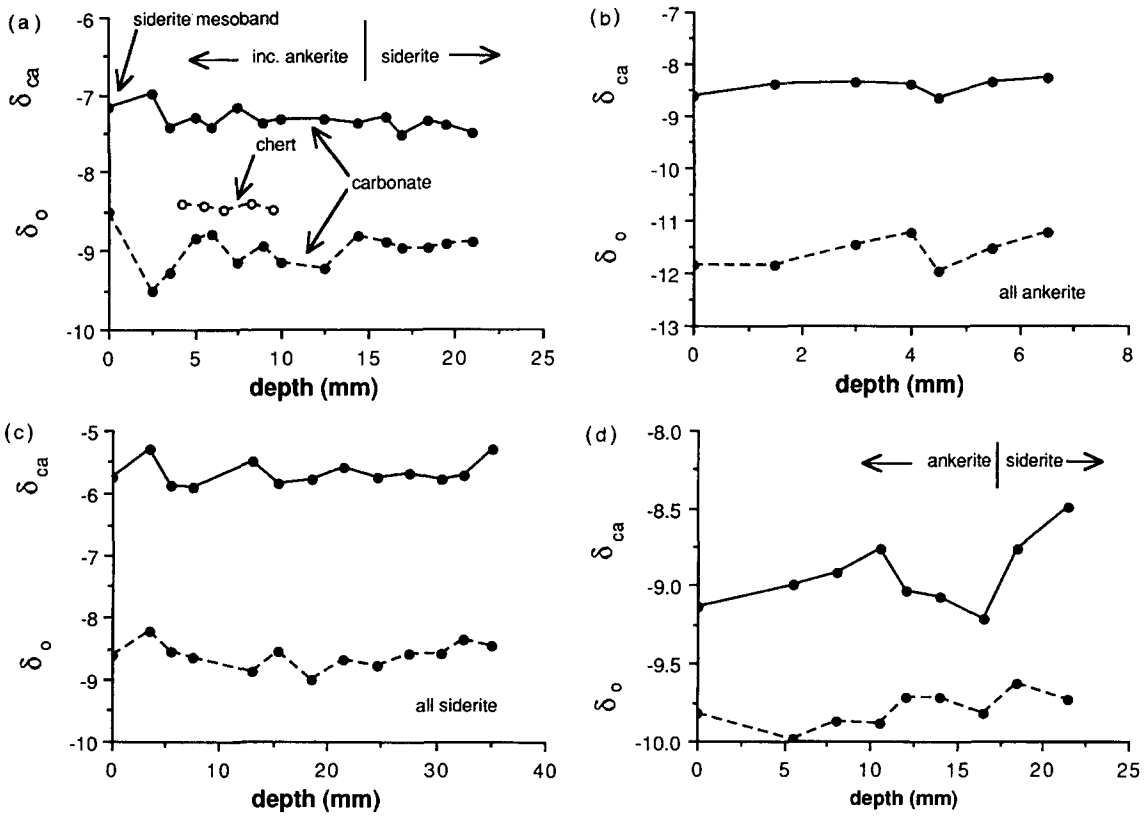

Fig. 3. Variation in $\delta^{13}C$ ($=\delta_{ca}$) and $\delta^{18}O$ ($=\delta_o$) of carbonate in successive microbands in a core segment from Pomfret drillhole AD-5 (a) 125.8 m and (b) 136.78 m, from Whitebank drillhole WB-98 (c) 268.8 m, and from Coretsi drillhole CN-109 (d) 189.07 m. Abundances of ^{18}O in chert microbands are also indicated in the core segment from (a) 125.8 m depth in the Pomfret drillhole.

corroborate the suggestion that temperatures in the zone of contact metamorphism did not significantly exceed 450°C.

4.2. Isotopic analysis

Following Beukes et al. (1990) the C-isotopic compositions of carbonate and total organic C are abbreviated as δ_{ca} and δ_{co} and the O-isotopic composition of the carbonates is abbreviated as δ_o in the text and figures. Lastly, ϵ is equal to $[(\delta_{ca}+1000)/(\delta_{co}+1000)-1]\times 1000$.

4.2.1. Isotopic temperatures

Temperatures in the aureole of contact metamorphism may be determined by O isotope thermometry if cherts and carbonates were isotopically equilibrated during the thermal event, and if subsequent events have not further altered the O-isotopic compositions of either phase. Oxygen-isotopic composi-

Notes to Table 3:

[a] Reported values represent means of duplicate measures. Uncertainties calculated as 95% confidence limits are 1.2%, 0.16‰, and 0.34‰ for % carbonate, δ_{ca}, and δ_o values, respectively.

[b] Vertical distance measurement on polished core segment relative to arbitrary zero point at center of first carbonate microband analyzed in each segment.

[c] Calculated from μmoles CO_2 per mg rock powder and approximate % of siderite ($FeCO_3$) or ankerite ($Ca_2MgFe(CO_3)_4$).

Table 3
Isotopic compositions of carbonate microbands in the Kuruman and Griquatown Iron Formations, South Africa [a]

Vertical distance[b] (mm)	% carbonate[c]	δ_{ca}(PDB)	δ_o(PDB)	δ_o(SMOW)
		(‰)		
	Pomfret drillhole AD-5, 125.8 m depth, n = 15			
0.0	99.4	-7.16	-8.96	21.62
2.5	82.6	-6.97	-9.97	20.58
3.5	24.5	-7.42	-9.75	20.81
5.0	29.5	-7.30	-9.29	21.28
6.0	32.8	-7.42	-9.25	21.33
7.5	35.7	-7.15	-9.60	20.96
9.0	26.9	-7.36	-9.41	21.16
10.0	41.9	-7.31	-9.61	20.95
12.5	38.8	-7.31	-9.68	20.88
14.5	15.5	-7.38	-9.27	21.30
16.0	20.3	-7.30	-9.35	21.22
17.0	11.6	-7.52	-9.43	21.14
18.5	26.5	-7.35	-9.42	21.15
19.5	20.0	-7.39	-9.37	21.20
21.0	30.0	-7.49	-9.35	21.22
	Pomfret drillhole AD-5, 132.84 m depth, n = 2			
0.0	33.0	-9.10	-10.54	20.00
3.0	25.2	-9.11	-10.69	19.84
	Pomfret drillhole AD-5, 136.78 m depth, n = 7			
0.0	6.8	-8.60	-11.86	18.63
1.5	14.6	-8.40	-11.84	18.66
3.0	16.7	-8.35	-11.47	19.04
4.0	14.8	-8.38	-11.23	19.28
4.5	9.4	-8.67	-11.95	18.55
5.5	4.9	-8.35	-11.53	18.98
6.5	28.2	-8.27	-11.24	19.28
	Whitebank drillhole WB-98, 882 m depth, n = 13			
0.0	21.2	-5.74	-9.06	21.52
3.5	57.5	-5.30	-8.69	21.90
5.5	15.8	-5.87	-9.00	21.58
7.5	38.5	-5.89	-9.10	21.48
13.0	44.5	-5.47	-9.33	21.24
15.5	35.0	-5.83	-9.02	21.56
18.5	26.5	-5.78	-9.47	21.10
21.5	38.7	-5.59	-9.14	21.44
24.5	35.7	-5.73	-9.24	21.34
27.5	40.7	-5.68	-9.05	21.53
30.5	38.2	-5.75	-9.04	21.54
32.5	40.4	-5.70	-8.83	21.76
35.0	50.9	-5.29	-8.91	21.68
	Coretsi drillhole CN-109, 189.07 m depth, n = 9			
0.0	19.9	-9.14	-10.28	20.26
5.5	66.0	-8.99	-10.44	20.10
8.0	35.8	-8.91	-10.33	20.21
10.5	43.1	-8.76	-10.35	20.19
12.0	43.9	-9.03	-10.19	20.36
14.0	35.8	-9.07	-10.17	20.38
16.5	57.1	-9.21	-10.28	20.26
18.5	51.7	-8.76	-10.09	20.46
21.5	55.4	-8.49	-10.19	20.36

tions of successive laminations of chert and carbonate in a sample from 125.8 m depth in the Pomfret drill core were used to estimate the temperature to which sediments 32 m away from the diabase sill were heated.

Chert microbands have constant $\delta^{18}O$ values of ~ 22.1 (Table 2; Fig. 3a). Samples of chert contain no admixed mineral phases except for iron carbonate, which was removed by acidification prior to O-isotopic analysis. The absence of band-to-band variations in 'pure' chert microbands suggests either that the primary precipitate was isotopically homogeneous, or that isotopic homogenization occurred after lithification. Intercalated carbonate microbands have δ_o values ranging from 21.0 to 21.3, and large band-to-band variations appear to be linked to the presence of diagenetic ankerite. Although samples from 21.0 to 12.5 mm are composed of pure siderite, the abundances of ankerite increases above 12.5 mm (where microbanded cherts were isolated). The sample from 2.5 mm is from a pure ankerite microband and the sample from 0.0 mm is from a siderite mesoband. Oxygen-isotopic compositions of ankerite-bearing microbands are slightly depleted in ^{18}O relative to pure siderite microbands.

The measured differences in O-isotopic composi-

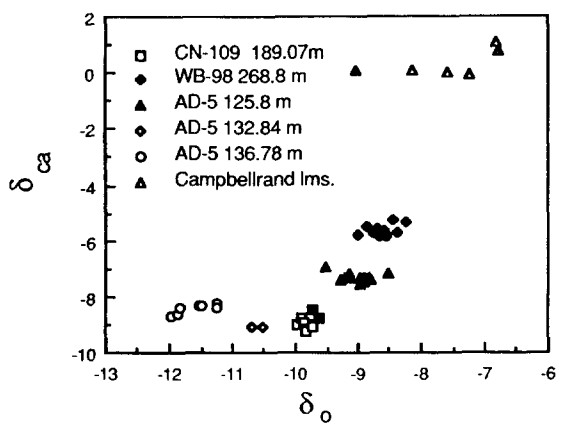

Fig. 4. Crossplot of δ_{ca} vs. δ_o in microbanded siderites and ankerites from the Kuruman and Griquatown Iron Formations. In samples from drillholes AD-5, WB-98, and CN-109 filled symbols represent siderite-rich microbands and open symbols represent ankerite-rich microbands. Isotopic compositions of microdrilled micrites and sparites (Beukes et al., 1990) from samples of Campbellrand carbonates are shown as open and half filled symbols, respectively.

tion between chert and siderite microbands Δ(QTZ–SID) values range from 0.8 to 1.4 with an average of ~ 1.0 (Table 2). When plotted on Fig. 4 of Becker and Clayton (1976), this isotopic difference corresponds to a temperature of ~ 250°C (range from 210 to 320°C) in sediments 32 m away from the diabase sill. Slightly higher temperatures are estimated if average $\delta^{18}O$ values of chert microbands are compared only with those of pure siderite microbands; in this case Δ(QTZ–SID) values are ~ 0.9 corresponding to a temperature of ~ 280°C. The small Δ(QTZ–SID) values determined in this study are most likely due to thermal re-equilibration of O between chert and siderite associated with contact metamorphism. Temperatures must have risen above 280°C towards the igneous sill (but not significantly above 450°C due to the persistence of iron-carbonate and stilpnomelane), and decreased to below 280°C below 125.8 m depth. In equivalent strata unaffected by contact metamorphism, Perry and Ahmad (1983) estimated temperatures ranging from 150 to 230°C from the magnitude of O isotope difference between chert and magnetite in whole-rock samples.

4.2.2. Microbanded carbonates

In addition to the section from 125.8 m depth, isotopic compositions of carbonates were determined in two sections from depths of 132.84 and 136.78 m in the Pomfret core, and in two other sections, one each from the Whitebank (882 m depth) and Coretsi (189.07 m depth) cores. The microbanded sample from Whitebank was collected in the Campbellrand–Kuruman transition zone (Beukes et al., 1990) underlying the Groenwater Member. The microbanded sample from Coretsi was collected in the Griquatown Iron Formation which conformably overlies the Kuruman Iron Formation.

Results of analyses of microbanded carbonates are listed in Table 3. Microbanded sequences from 132.84 and 136.78 m (Fig. 3b) in the Pomfret core are composed of successive laminations of ankerite and minnesotaite-rich chert. In contrast, microbanded sequences from 125.8 m (Fig. 3a) in the Pomfret core and 882 m (Fig. 3c) in the Whitebank core are composed of successive laminations of siderite and 'pure' chert. In the sample from 189.07 m (Fig. 3d) in the Coretsi core, two mineralogic zones are apparent. One contains thick laminations of ankerite with

minnesotaite in matrix cherts; the second contains thinner siderite laminations in a greenalite-rich matrix with minor ankerite rhombohedra. Band-to-band variations in ^{13}C and ^{18}O abundances of carbonates are small, typically less than 0.3‰. The magnitudes of these band-to-band variation are similar to those determined for carbonate microbands from the Dale Gorge Member BIF (Kaufman et al., 1990).

In general, iron-rich carbonates in all microband sequences are depleted by 5 to 9‰ in ^{13}C and by 1 to 5‰ in ^{18}O relative to open marine, stromatolitic limestones of the underlying Campbellrand Formation (Fig. 4). Carbon- and O-isotopic compositions of ankerite microbands are typically depleted relative to siderite microbands. In fact, isotopic depletion in microbanded carbonates appears to correlate with diagenetic replacement of fine-grained siderite by coarse-grained ankerite (cf. Kaufman et al., 1990; Winter and Knauth, 1992). Siderites from unaltered or only slightly altered microband sequences from 125.8 m in the Pomfret core and 882 m in the Whitebank core are most enriched in both ^{13}C and ^{18}O; whereas ankerites from altered microband sequences from 132.84 and 136.78 m in the Pomfret core are most depleted in both isotopes. In the microband sequence from the Coretsi core, siderites are slightly more enriched in both isotopes relative to ankerites isolated from the same sample. Petrographic relationships suggest that ankerite does replace pre-existing siderite; this must have occurred in the presence of Ca^{2+}- and Mg^{2+}-rich solutions. From results of this study and the study of microbanded carbonates in the Dales Gorge Member (Kaufman et al., 1990; see also Winter and Knauth, 1992 for similar results in the Gunflint Iron Formation) it seems that these solutions were also depleted in both ^{13}C and ^{18}O, resulting in the formation of coarse-grained ankerite with isotopic compositions depleted relative to those of residual siderite. Depletion of ^{13}C in diagenetic waters possibly occurred through thermally mediated degradation of organic carbon during diagenesis (Beukes et al., 1990).

4.2.3. Mesobanded carbonates

Results of isotopic analyses of mesobanded carbonates in one of the sedimentary cycles present in the Groenwater Member (Cycle 3; 132.5 to 137.0 m in the Pomfret AD-5 core) are presented in Table 4. Cycle 3 was chosen for detailed analysis because all lithologies in the stilpnomelane lutite ferhythmite macrocycle are represented and because it was originally assumed that these sediments were deep enough in the AD-5 core to avoid most effects of contact metamorphism.

Isotopic compositions of mesobanded carbonates are illustrated in Fig. 5. Carbon-13 abundances range from -7.5 to -13.1 while δ_o values range from -9.3 to -12.7. Samples of siderite microsparite from mesobands in the intraclastic chert facies (136.90 m depth) are the most enriched in ^{13}C and show no evidence of replacement by magnetite. In contrast, samples of siderite microsparite from mesobands and microbands in all other facies are depleted in ^{13}C relative to samples from the intraclastic chert facies and do show evidence of replacement by magnetite. This observation suggests that formation of magnetite by oxidation of siderite somehow resulted in more negative and variable C-isotopic compositions in the residual siderite. This may be a function of the incorporation of C, into newly formed siderites, from the oxidation of co-existing organic matter. Alternatively, it is plausible to suggest that some factors (perhaps related to primary environmental variations associated with high rates of evaporation or isotopic variations associated with water depth) resulted in primary siderite C-isotopic compositions that have varied between BIF facies.

Mesobands containing rhombohedral ankerite in the minnesotaite-rich siderite-microbanded chert facies (136.78 m depth) exhibit the greatest degree of ^{13}C depletion ($\delta_{ca} = -12$ to -13). The presence of cryptalgal laminations in these samples indicates that mat-building organisms were present and probably provided an additional source of organic C to the sediments. It seems possible that oxidation (during burial metamorphism) of originally organic-rich facies resulted in the formation of ankerite more depleted in ^{13}C than that in organic-poor facies.

4.3. Elemental and isotopic analyses of whole-rock samples

4.3.1. Stratigraphic variations

Abundances and isotopic compositions of carbonates and TOC, and abundances of selected major elements are presented in Table 5. Lithologic, iso-

Table 4
Abundance and isotopic compositions of mesobanded carbonates in sedimentary Cycle 3 from the Groenwater Member of the Kuruman Iron Formation

sample	% carbonate[a]	δ_{ca}(PDB)	δ_o(PDB)	δ_o(SMOW)
			(‰)	
132.84A-1	78.8	-8.93	-11.10	19.42
-2	73.1	-9.52	-10.40	20.14
-3	90.9	-8.86	-10.57	19.96
-4	45.9	-9.24	-10.66	19.87
-5	68.6	-8.95	-10.80	19.73
-6	55.0	-9.15	-10.09	20.46
132.84B-1	84.3	-10.63	-10.24	20.30
-2	31.6	-10.27	-9.88	20.67
-3	14.2	-10.78	-10.06	20.49
-4	19.0	-9.66	-10.47	20.07
-5	2.3	-10.24	-10.83	19.70
-6	20.4	-9.62	-10.14	20.41
-7	67.1	-10.46	-9.88	20.67
132.84C-1	19.4	-9.10	-10.74	19.79
-2	43.5	-9.62	-10.84	19.69
-3	36.7	-9.36	-10.51	20.03
-4	68.2	-9.78	-10.77	19.76
-5	72.5	-9.67	-9.97	20.58
-6	40.6	-9.74	-9.82	20.74
-7	8.2	-9.58	-10.36	20.18
-8	17.2	-9.96	-9.64	20.92
-9	59.8	-10.46	-9.84	20.72
132.84D-1	32.3	-10.02	-10.45	20.09
-2	21.0	-10.90	-9.76	20.80
-3	53.5	-10.30	-9.88	20.68
-4	66.5	-10.01	-10.27	20.27
-5	44.7	-10.47	-9.59	20.97
-6	6.7	-10.73	-10.18	20.36
133.15A-1	10.5	-9.99	-11.51	19.00
-2	16.2	-9.80	-11.45	19.06
-3	8.5	-9.55	-11.54	18.96
-4	15.3	-10.18	-9.82	20.73
133.15B-1	1.9	-11.10	-10.71	19.82
-2	13.0	-10.19	-10.16	20.39
134.41A-1	56.9	-10.42	-11.05	19.47
-2	37.7	-10.56	-9.25	21.32
-3	34.3	-10.33	-10.21	20.34
-4	33.8	-10.30	-9.51	21.06
-5	56.4	-10.55	-10.55	19.98
-6	20.9	-10.47	-10.76	19.77
134.41B-1	17.5	-10.61	-10.80	19.73
-2	4.8	-10.43	-10.90	19.62
-3	8.4	-10.42	-11.31	19.20
-4	3.2	-10.58	-10.66	19.88

Table 4 (continued)

sample	% carbonate[a]	δ_{ca}(PDB)	δ_o(PDB)	δ_o(SMOW)
			(‰)	
135.60-1	3.8	-10.55	-11.24	19.26
-2	10.8	-10.80	-10.27	20.27
-3	7.7	-10.73	-10.76	19.77
-4	6.7	-10.77	-10.55	19.99
-5	12.6	-10.85	-9.56	21.00
136.55-1	18.9	-9.61	-10.86	19.67
-2	10.9	-9.85	-10.94	19.58
-3	4.9	-9.39	-10.24	20.31
-4	15.5	-9.87	-11.18	19.34
-5	5.7	-9.63	-11.53	18.98
-6	15.5	-9.86	-9.47	21.08
-7	12.1	-9.54	-9.63	20.94
-8	6.0	-9.93	-11.25	19.27
136.78A-1	53.8	-9.19	-10.90	19.62
-2	68.3	-9.39	-10.16	20.38
-3	74.8	-9.40	-10.53	20.00
-4	69.4	-9.48	-10.19	20.36
-5	58.9	-9.50	-10.04	20.51
136.78B-1	82.9	-9.41	-10.91	19.61
-2	91.2	-9.03	-10.61	19.93
-3	66.8	-9.97	-9.69	20.87
-4	28.9	-10.00	-9.60	20.96
-5	40.6	-9.90	-9.93	20.62
136.78C-1	4.9	-13.11	-12.72	17.75
-2	61.9	-10.30	-11.93	18.56
-3	46.4	-12.63	-12.03	18.46
-4	43.4	-12.74	-12.18	18.31
-5	4.8	-12.79	-12.35	18.13
136.90A-1	41.3	-8.31	-10.57	19.96
-2	42.3	-7.46	-10.53	20.00
-3	29.2	-8.21	-11.03	19.49
-4	81.3	-8.61	-11.30	19.21
-5	20.5	-8.74	-11.66	18.84
136.90B-1	87.5	-8.73	-10.73	19.80
-2	55.9	-8.59	-10.58	19.95
-3	30.5	-8.22	-10.65	19.88
-4	14.6	-7.95	-11.08	19.44
-5	40.1	-8.23	-10.54	19.99
136.90C-1	1.2	-8.99	-10.87	19.66
-2	32.2	-9.24	-11.07	19.45
-3	43.8	-8.55	-10.04	20.51

[a] Determined from yield of CO_2 after phosphorlysis and visual estimate of the ratio of siderite to ankerite after staining and petrographic analysis.

topic (δ_{ca} and δ_{co}), and elemental (%Fe and Fe^{2+}/total Fe) variations in the four stilpnomelane lutite ferhythmite macrocycles are graphically summarized in Fig. 6. Cycle 1 (Fig. 6a) represents the most condensed section, spanning only 1 m in thickness, yet displays the most distinct isotopic and

Table 5
Abundance and isotopic composition of carbonate and total organic carbon with partial elemental analyses of whole-rock samples in sedimentary cycles from the Groenwater Member of the Kuruman Iron Formation

Depth (m)	Facies[a]	Carbonate				TOC		ε^c (‰)	Al_2O_3	FeO[d]	P_2O_5	S	Fe^{2+}/total Fe
		%[b]	δ_o(PDB) (‰)	δ_o(PDB) (‰)	δ_o(SMOW) (‰)	mgC/g	δ_{co}(PDB) (‰)		(wt. %)				
95.90	St	2.51	-14.8	-12.4	18.1	1.87	-40.4	26.7		58.11		0.54	0.36
95.98	CA	0.73	-14.2	-11.4	19.1	0.72	-35.8	22.4		34.16		0.02	0.89
96.11	BMi	0.19	-14.2	-12.1	18.4	0.33	-35.5	22.1		42.45		0.01	0.55
96.25A	BMi/A	0.47	-12.1	-12.6	17.9	0.45	-35.4	24.2	0.15	49.03	0.15	0.02	0.51
B	BMi		-13.4	-13.9	16.5	0.42	-33.6	20.9	0.04	36.16	0.78		0.62
96.40A	BMi/A	0.37	-12.1	-14.3	16.1	1.15	-34.7	23.4	0.17	35.39	0.48	0.02	0.62
B	SC		-11.7	-12.9	17.5	11.88	-28.8	17.6	0.17	25.74	0.01		0.80
C	BMi					0.16	-31.5		0.06	22.52	0.01		0.89
96.53A	BMi	0.89	-9.8	-12.9	17.6	0.66	-31.1	22.0	0.13	27.80	0.01	0.11	0.89
B	BMi		-11.1	-13.7	16.7	1.09	-34.9	24.7	0.19	22.01	0.01		0.84
96.63	St	2.00	-11.0	-12.1	18.4	9.16	-36.2	26.1		37.25		0.76	0.72
96.89	BMi/A	5.59	-11.9	-13.0	17.5	0.51	-35.0	23.9		14.25		0.03	0.91
112.02	CA	1.69				0.10	-28.4			7.05		0.14	0.63
112.40	BMi	0.05	-13.2	-12.6	17.9	0.10	-27.8	15.0		43.19		0.01	0.56
112.88	BMi/A	0.28	-12.0	-10.9	19.6	0.08	-29.9	18.5		40.12		0.01	0.56
113.22A	BMi/A	0.98	-10.7	-11.9	18.6	0.42	-29.8	19.7	0.05	34.11	0.15	0.02	0.68
B	BMi/A		-11.9	-11.9	18.6	0.60	-31.0	19.7	0.07	38.48	0.34		0.73
C	BMi/A		-11.7	-9.9	20.6	0.21	-32.6	21.6	0.07	20.08	0.15		0.88
113.50	St	0.97	-10.5	-11.4	19.1	11.75	-37.4	27.9		36.11		0.08	0.66
113.73A	BS	4.55	-10.6	-12.1	18.4	0.16	-29.4	19.4	0.10	23.55	0.32	1.16	0.86
B	BS		-10.2	-13.0	17.5	0.35	-32.2	22.7	0.08	6.18	0.10		0.83
114.23A	CS	2.55	-10.3	-11.5	19.0	0.14	-23.4	13.4	0.08	37.19	0.01	0.22	0.85
B	BS		-10.3	-12.1	18.4	0.54	-28.4	18.6	0.14	26.13	0.27		0.75
C	BS		-10.4	-11.2	19.3	0.16	-26.4	16.4	0.09	32.56	0.01		0.89
114.56	BMi	3.90	-13.2	-10.9	19.6	0.20	-25.7	12.8		36.67		0.09	0.37
132.66	St	0.61	-11.2	-14.1	16.3	0.25	-28.0	17.3		32.81		0.12	0.56
132.84	BS	1.10	-9.9	-11.2	19.3	0.08	-29.0	19.7		30.23		0.02	0.72
133.15	BM/H	3.94	-10.1	-10.6	20.0	0.13	-26.2	16.5		38.21		0.02	0.29
134.41	BM/H	1.04	-10.7	-11.4	19.1	0.16	-26.4	16.1		45.46		0.04	0.24
135.60	BM/H	1.47	-11.4	-10.6	19.9	0.16	-26.5	15.5		51.73		0.05	0.29
136.50	BH	0.20				0.15	-25.1		0.04	41.80	0.12	0.01	
136.55	BM/H	5.87	-9.6	-10.6	20.0	0.23	-26.4	17.3		38.96		0.01	0.38
136.78	BMi	0.91	-9.3	-10.4	20.1	0.16	-27.4	18.6		33.31		0.03	0.72
136.90	MS	3.32	-8.4	-11.4	19.1	0.17	-25.3	17.3		13.81		0.14	0.92
137.00	St	3.34				0.27	-26.2			30.67		0.11	0.64
140.93A	BS	0.52	-10.5	-12.8	17.7	0.22	-22.7	12.5	1.90	33.85	0.08	0.02	0.71
B	BS		-9.9	-13.2	17.3	0.19	-21.2	11.5	0.05	7.59	0.01		0.98
141.10	CA	4.91	-9.3	-11.3	19.2	0.18	-24.4	15.5		40.44		0.02	0.41
141.62	BM/H	1.66	-9.6	-11.1	19.4	0.09	-26.7	17.6		45.16		0.01	0.29
142.75A	BMi	0.76	-11.0	-13.0	17.5	0.22	-25.0	14.6	0.52	43.76	0.16	0.01	0.37
B	BMi		-10.5	-11.4	19.1	1.53	-27.8	17.8	0.19	55.60	0.30		0.35
C	BMi		-10.9	-12.2	18.2	0.63	-28.1	7.3	0.10	19.56	0.26		0.52
143.90	BMi	0.78	-12.0	-10.9	19.7	0.08	-31.0	19.6		39.42		0.01	0.61
144.04	BS	1.75	-12.6	-11.2	19.3	0.18	-30.5	18.5		35.88		0.01	0.86
144.12A	CS	3.57	-11.3	-13.2	17.2	0.34	-23.9	12.9	2.33	43.11	0.15	0.08	0.40
B	BS		-10.7	-12.7	17.7	0.22	-24.4	14.0	0.08	13.00	0.01		0.93
C	BS					0.08	-22.9		0.11	18.40	0.13		0.93

[a] Facies codes as defined by Beukes et al. (1990): B = BIF; M = magnetite-rich; Mi = minnesotaite-rich (in addition to magnetite); H = hematite-rich (in addition to magnetite); S = siderite; CS = sideritic chert; CA = ankeritic chert; MS = sideritic micrite; SC = carbonaceous shale; A = cryptalgal; St = stilpnomelane lutite.
[b] Total C (determined by LECO method or by coulometric titration)—TOC
[c] $\epsilon = [(\delta_{ca} + 1000)/(\delta_{co} + 1000) - 1] \times 1000$.
[d] Total Fe as FeO.

elemental variations. Effects of contact metamorphism are most evident in this cycle. From the base to the top of Cycle 1, a general trend towards more negative δ_{ca} values, increase in abundance of total Fe (as FeO), and increase in oxidation state of Fe (Fe^{2+}/total Fe) is noted. Abundances of total carbonate and TOC are low in all samples except stilpnomelane lutites and an organic-rich shale (Table 5). Carbon-13 abundances in TOC are variable. The most negative δ_{co} values are associated with samples of stilpnomelane lutite and an organic-rich shale, whereas the most positive is associated with a sample of organic-rich shale (Table 5; Fig. 6a). The increase in total Fe near the igneous intrusion is attributed to enhanced infiltration and mixing of Fe-rich fluids and high-temperature formation of minnesotaite and magnetite. Variation in oxidation state of samples is controlled by the relative abundance of iron-bearing minerals. In Cycle 1, the decrease in Fe^{2+}/total Fe is associated with an increase in abundance of magnetite and hematite relative to iron-bearing carbonates. The massive chert from 95.98 m depth is almost totally replaced by minnesotaite but contains no magnetite or hematite. A general decrease in δ_{ca} values in the transition from siderite- to oxide-rich BIF has been correlated with an increase in abundance of ^{13}C-depleted ankerite formed during deep burial diagenesis (Beukes et al., 1990). The distinct trends continue through several different lithologies in Cycle 1 (including siderite- and oxide-rich BIF) indicating that heating of these sediments during contact metamorphism caused additional depletion of ^{13}C in residual carbonates (Fig. 6a).

Similar trends in isotopic and elemental abundances are not evident in Cycles 2, 3, and 4 (Figs. 6b, 6c, and 6d). In BIF sediments more than 10 m from the igneous sill, lithologic variations apparently exert predominant control over isotopic and elemental abundances. In Cycles 2, 3, and 4, δ_{ca} values are relatively constant, with more negative values commonly associated with oxide-rich BIF and more positive values commonly associated with siderite-rich BIF or chert. Wide variations in δ_{co} values are the most distinct features of Cycles 2 and 4. The extreme ^{13}C depletion in TOC from an organic-rich sample of stilpnomelane lutite at 113.50 m (Fig. 6b; $\delta_{co} = -37.4$) is of particular significance in understanding

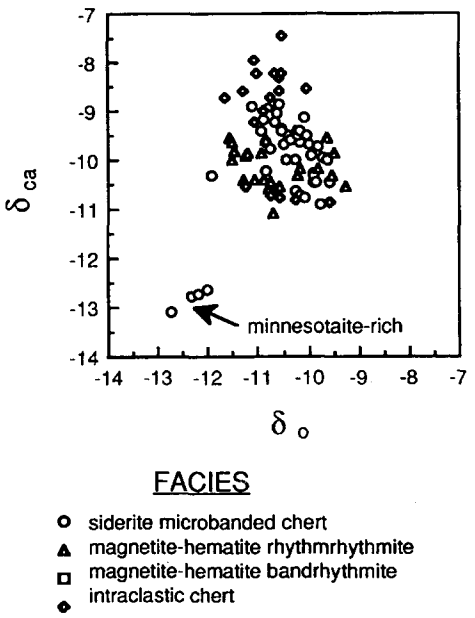

Fig. 5. Crossplot of δ_{ca} vs. δ_o in mesobanded carbonates from Cycle 3 (132.5 to 137 m depth in the Pomfret AD-5 core) in the Groenwater Member of the Kuruman Iron Formation.

the origin of this facies. The isotopic composition of this sample is similar to that in organic-rich samples from stilpnomelane lutite beds at 95.98 m ($\delta_{co} = -40.4$) and 96.63 m ($\delta_{co} = -36.2$) in Cycle 1 (Fig. 6a). In contrast, two organic-poor samples from stilpnomelane lutite beds at 132.66 and 137.00 m in Cycle 3 (Fig. 6c) have relatively enriched isotopic compositions ($\delta_{co} = -28.0$ and -26.2, respectively). Wide variations in the abundance and C-isotopic compositions of total organic C in similar lithofacies suggest that two independent depositional processes may have led to the formation of stilpnomelane lutites in BIF sediments. The presence of axiolitic shard-like textures in *massive* stilpnomelane lutite beds has been interpreted by LaBerge (1966) as indicative of a pyroclastic origin for these units. However, other *thinner* stilpnomelane lutite beds, lacking shard-like structures and commonly containing abundant siderite, magnetite, chert, and occasionally apatite, appear to have a detrital origin. Isotopic analyses suggest that massive, organic-rich stilpnomelane lutites with δ_{co} values near -36 are derived from a volcanic source, while thinner,

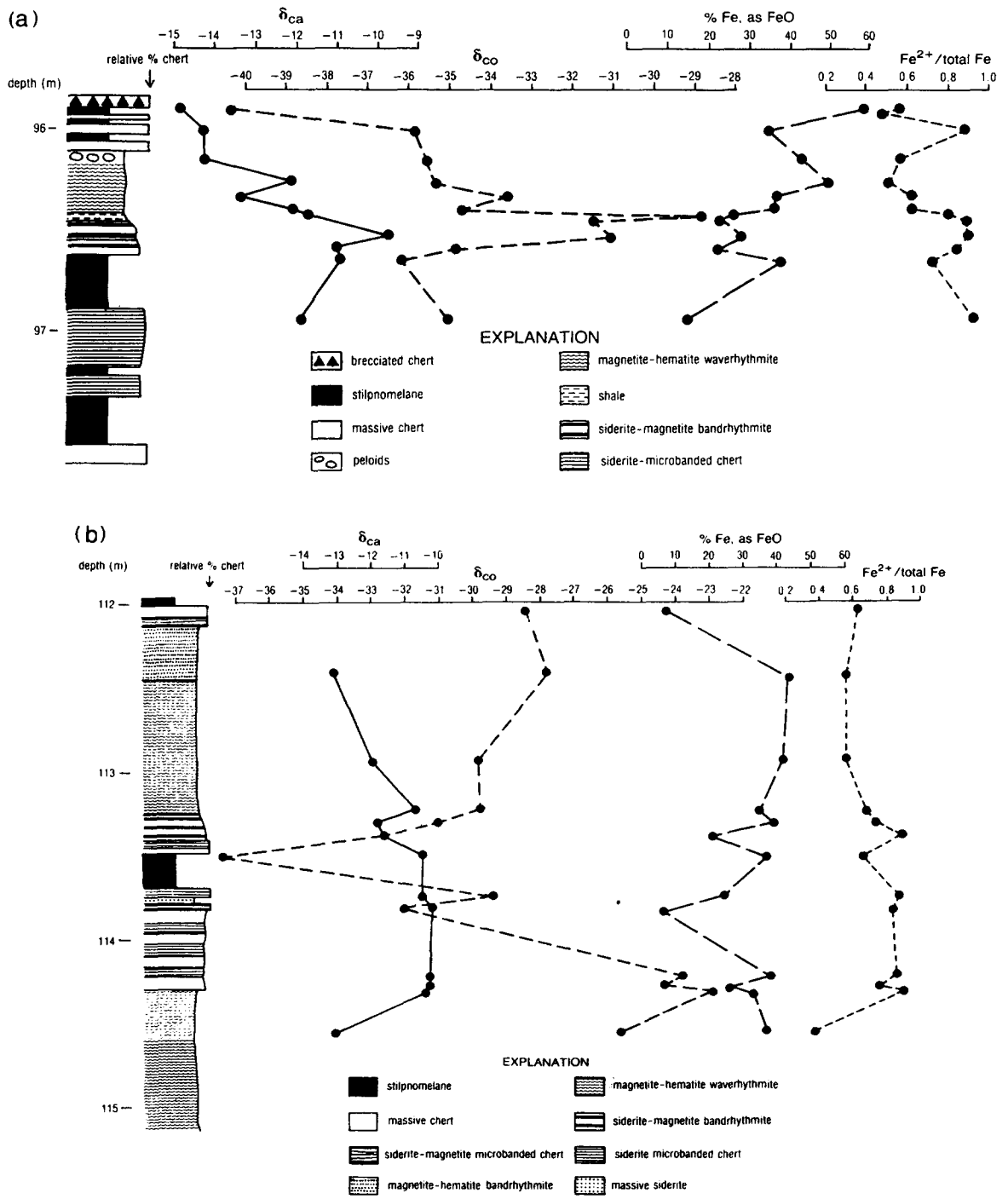

Fig. 6. Lithologic, isotopic [δ_{ca} vs. δ_{co} ($= \delta^{13}C_{\text{Total Organic Carbon}}$)], and elemental (% Fe and Fe^{2+}/total Fe) variations in stilpnomelane lutite ferhythmite macrocycles from (a) Cycle 1, (b) Cycle 2, (c) Cycle 3 and (d) Cycle 4 in the Groenwater Member of the Kuruman Iron Formation.

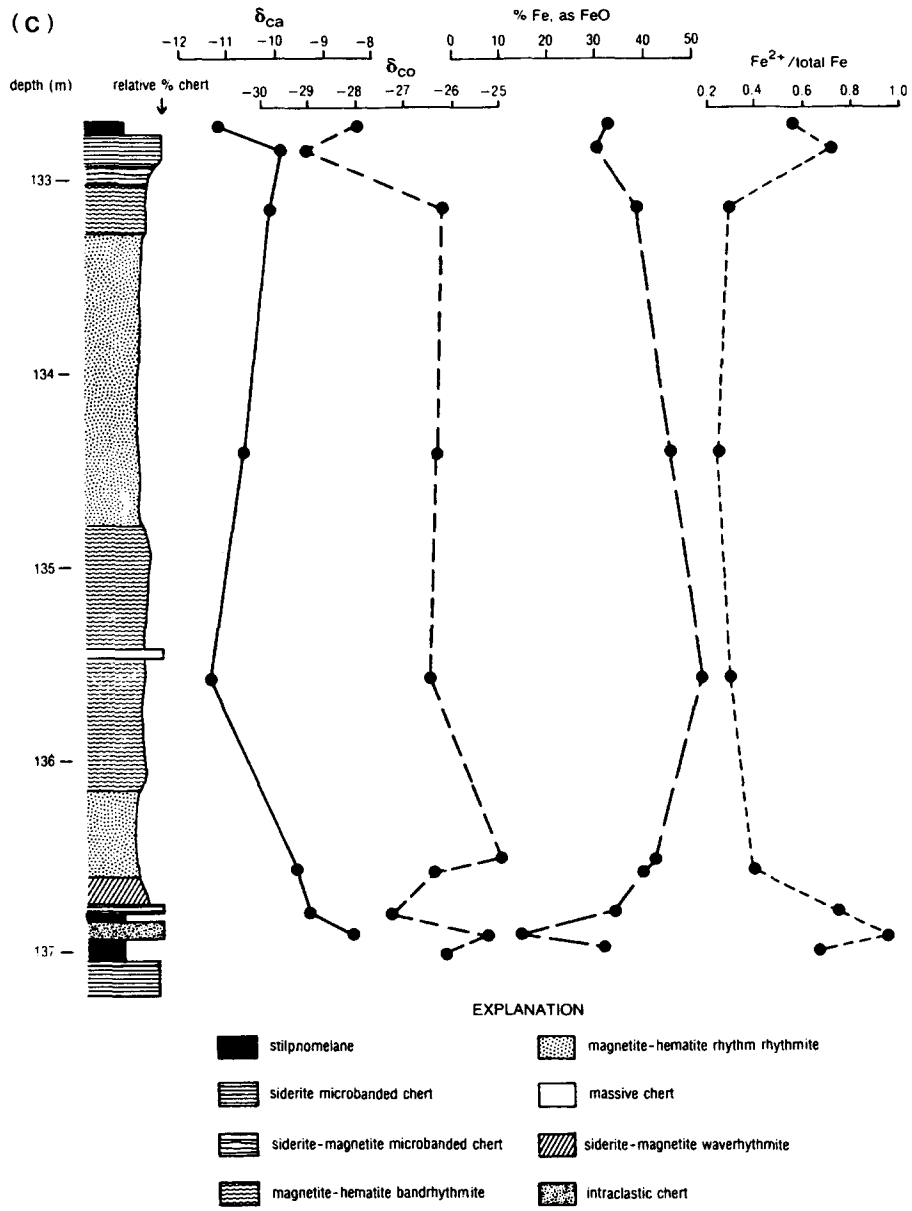

Fig. 6 (continued).

organic-poor stilpnomelane lutites with δ_{co} values near −25 have a detrital source. Detailed petrographic and isotopic studies of numerous stilpnomelane lutite beds should help to clarify this question.

Contrasting with extreme depletion of δ_{co} in the sample of stilpnomelane lutite in Cycle 2, δ_{co} in samples from underlying siderite- and oxide-rich BIF are markedly enriched (Fig. 6b). Above the stilpnomelane lutite, δ_{co} values in samples of siderite- and oxide-rich BIF are again enriched, but not to the

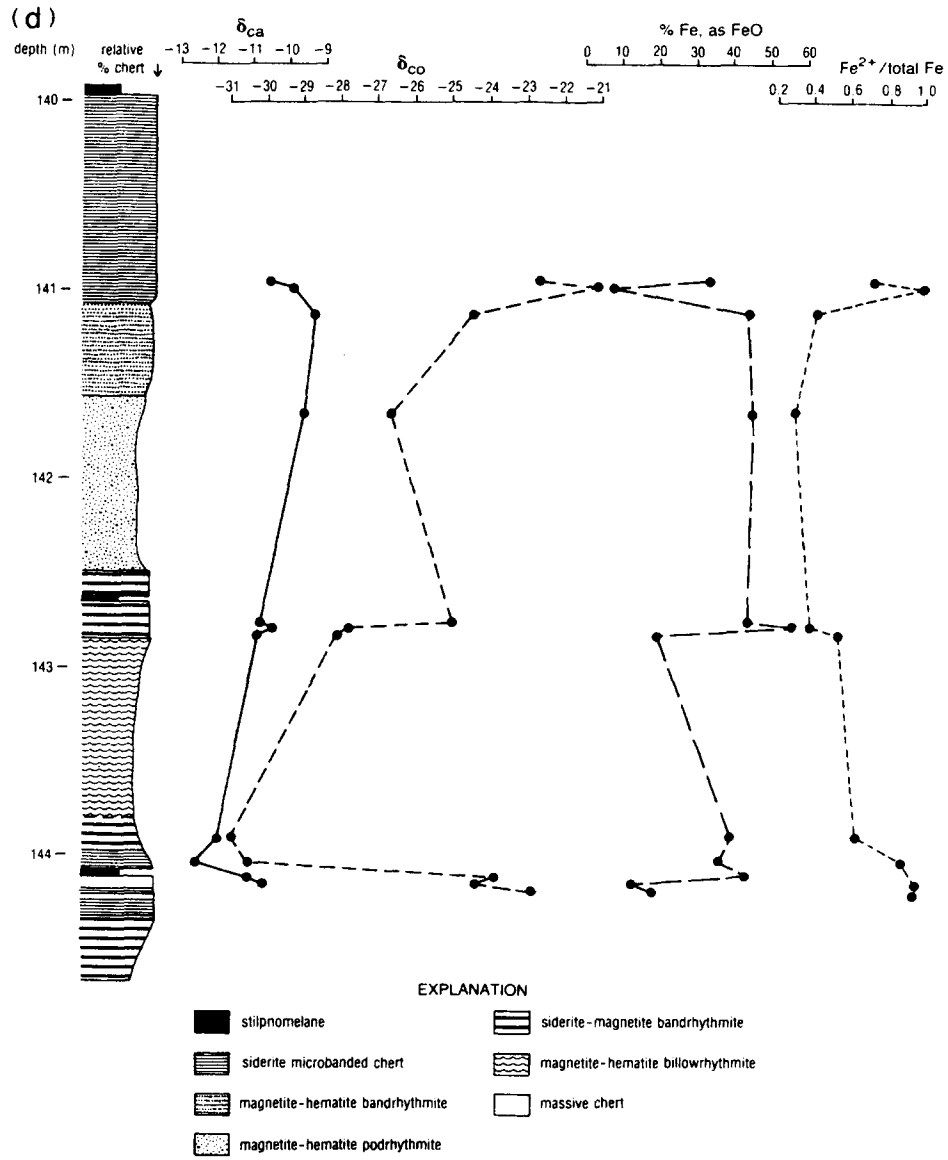

Fig. 6 (continued).

same degree. A similar isotopic excursion straddles a thin stilpnomelane lutite bed near the base of Cycle 4 (Fig. 6d). The variation in δ_{co} between similar lithologies above and below stilpnomelane lutite beds is not well understood. Abundances of organic C and total Fe as well as oxidation state of Fe in these samples are similar. Further, there is no independent evidence indicating that sources of organic C preceding and postdating stilpnomelane lutite beds were different. Beukes (1983, 1984), however, suggests that volcanic activity associated with the deposition of stilpnomelane lutite layers led to temporary toxic conditions for organisms. If correct, the elimination of most primary producers in the basin would likely

change the source (and isotopic composition) of organic C to sediments above volcanic layers.

4.3.2. Isotopic and elemental contrasts related to contact metamorphism

Correlations of C-isotopic abundances (δ_{ca}, δ_{co}, ϵ) with δ_o, isotopic abundances (δ_{ca}, δ_{co}, ϵ, and δ_o) with abundances of TOC and total Fe (as FeO), and abundances of TOC with total Fe (as FeO) in whole-rock samples from the Groenwater Member are presented, respectively, in Figs. 7, 8 and 9, and 10. Abundances of ^{13}C and ^{18}O in whole-rock carbonate samples from the Groenwater Member are depleted relative to similar samples in the underlying Campbellrand–Kuruman transition zone. For example, samples of siderite-rich BIF (the most abundant lithologic type common to both sequences) in the Groenwater Member have δ_{ca} values ranging from -10 to -12 and δ_o values ranging from -8 to -11 while similar samples in the underlying transition zone have δ_{ca} values ranging from -4 to -8 and δ_o values ranging from -11 to -13 (Fig. 7a). Differences in isotopic compositions of carbonates from similar facies (i.e., siderite-rich BIF) suggest that samples from the Groenwater Member in the AD-5 drillhole have been altered by contact metamorphism. In fact, systematic depletion of ^{13}C and ^{18}O is typical of siliceous limestones and dolomites which have been altered by contact metamorphism (see review by Valley, 1986 and references cited

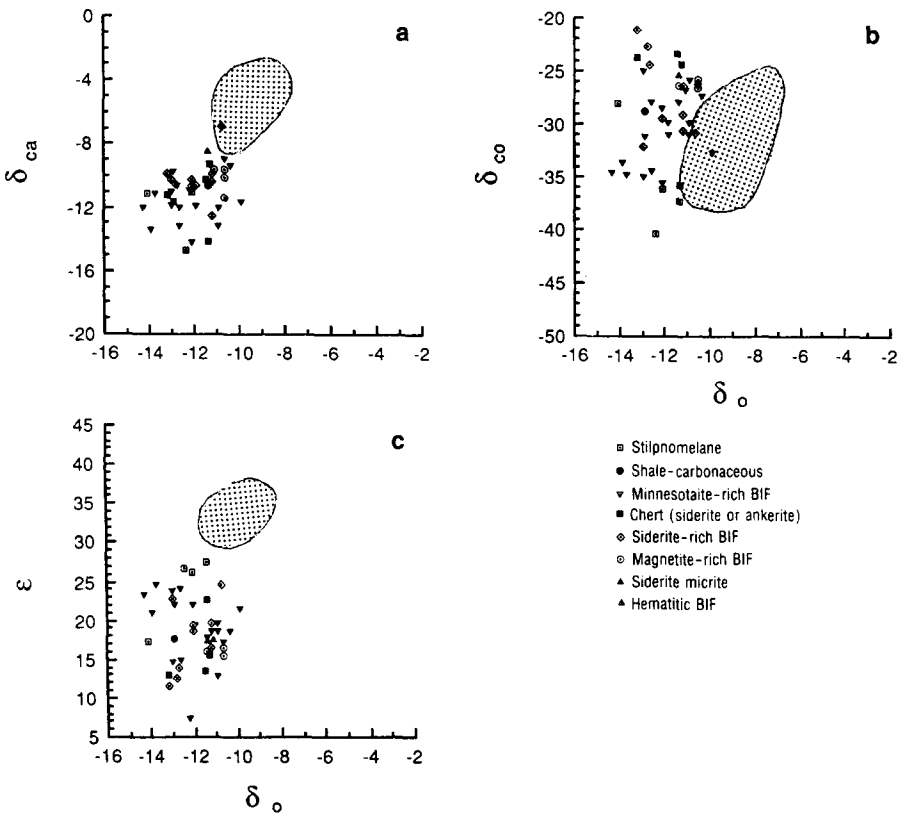

Fig. 7. Crossplots of δ_o vs. δ_{ca}, δ_{co}, and ϵ ($=\delta_{ca}-\delta_{co}$) in whole-rock samples from various lithofacies in the zone of contact metamorphism within the Groenwater Member of the Kuruman Iron Formation. Stippled region represents isotopic range of siderite-rich BIF samples from similar lithofacies in the underlying Campbellrand–Kuruman transition zone (cf. Beukes et al., 1990).

therein). As the degree of metamorphism increases, values of $\delta^{13}C$ and $\delta^{18}O$ decrease.

Organic C from siderite-rich BIF is generally enriched in ^{13}C relative to that in the underlying transition zone (Fig. 7b, 8b, and 9b). This is likely due to thermal alteration accompanying contact metamorphism. Lower abundance of TOC in samples of siderite-rich BIF relative to similar samples outside of the metamorphic aureole (Figs. 8 and 10) is consistent with this interpretation. Organic-rich samples of stilpnomelane lutite and shale exhibit the lowest δ_{co} values. Minnesotaite-bearing, oxide-rich BIF samples have a wide range of δ_{co} values, but are generally less enriched than siderite-rich BIF samples and contain slightly more organic C (Fig. 8b). Present results suggest that organic C in chert-rich (oxide-poor) BIF was more effectively oxidized during contact metamorphism than that in oxide-rich BIF, an observation consistent with metamorphic reactions leading to the formation of minnesotaite in chert-rich facies.

Due to greater depletion of ^{13}C in carbonate and greater enrichment of ^{13}C in TOC, ϵ values in samples from the Groenwater Member are typically smaller than those from similar lithologies in the underlying transition zone (Figs. 7c, 8c, and 9c). This may reflect the exchange of C-isotopic species between carbonate and organic C during contact metamorphism (Valley and O'Neil, 1981). Beukes et al. (1990) suggest that the metamorphic aureole in

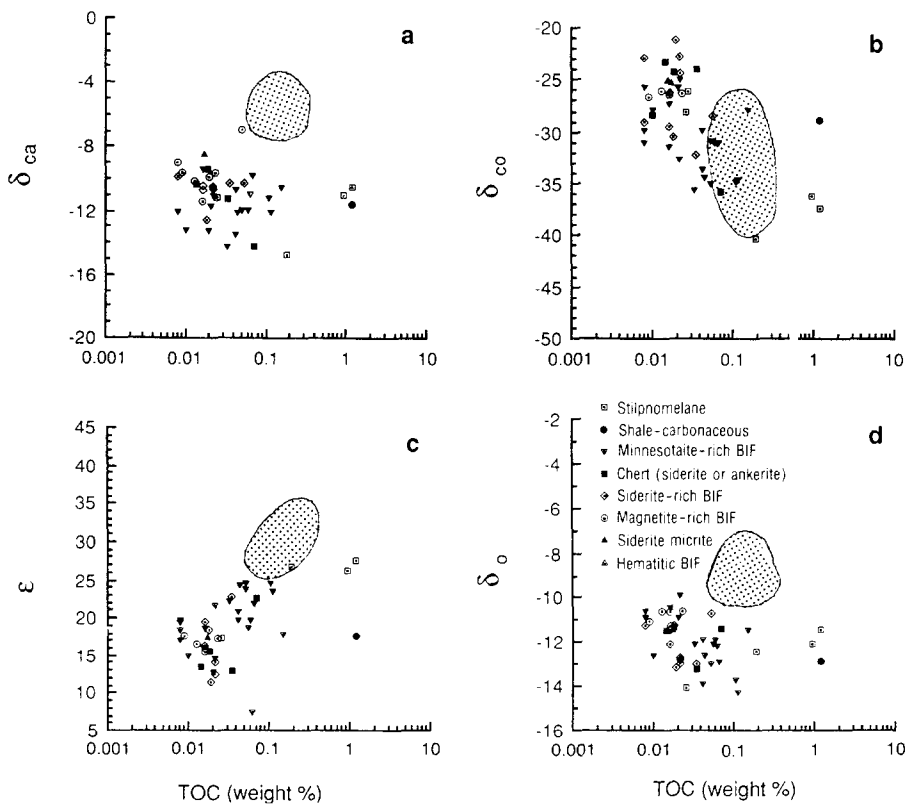

Fig. 8. Crossplots of abundance of TOC vs. δ_o vs. δ_{ca}, δ_{co}, and ϵ in whole-rock samples from various lithofacies in the zone of contact metamorphism within the Groenwater Member of the Kuruman Iron Formation. Stippled region represents the range of abundance of TOC and isotopic composition of siderite-rich BIF samples from similar lithofacies in the underlying Campbellrand–Kuruman transition zone.

the Pomfret core extends to about the 125 m depth in the AD-5 drillhole. But, reduced ϵ values in samples down to the 160 m depth (see fig. 6a of Beukes et al., 1990) suggest that the effect of contact metamorphism may extend at least to that level.

The abundance of total Fe is similar in samples of siderite-rich BIF from both the Groenwater Member and from the underlying transition zone (Figs. 9 and 10). Oxidation state of Fe (Fe^{2+}/total Fe) is correlated with abundance of total Fe (Fig. 11), but there is no apparent correlation between the oxidation state of Fe (or abundance of total Fe) and C-isotopic compositions of whole-rock samples. Only in samples very close to the diabase sill have the effects of enhanced fluid infiltration and circulation caused an increase in the abundance of iron.

Conclusions

Mineralogic and isotopic compositions of BIF samples from the Groenwater Member of the Kuruman Iron Formation, South Africa have been altered by contact metamorphism associated with intrusion of a diabase sill. Within the metamorphic aureole, minnesotaite was formed by reaction of siderite with chert or by dehydration of greenalite. The abundance of iron carbonates decreases towards the igneous sill, but trace amounts of primary and early diagenetic (pre-intrusion) carbonate and stilpnomelane remain in samples as close as 4 m from the sill, suggesting that temperatures did not exceed 450°C. In sediments 32 m away from the intrusion, a temperature of ~ 280°C is suggested by oxygen-isotopic differences

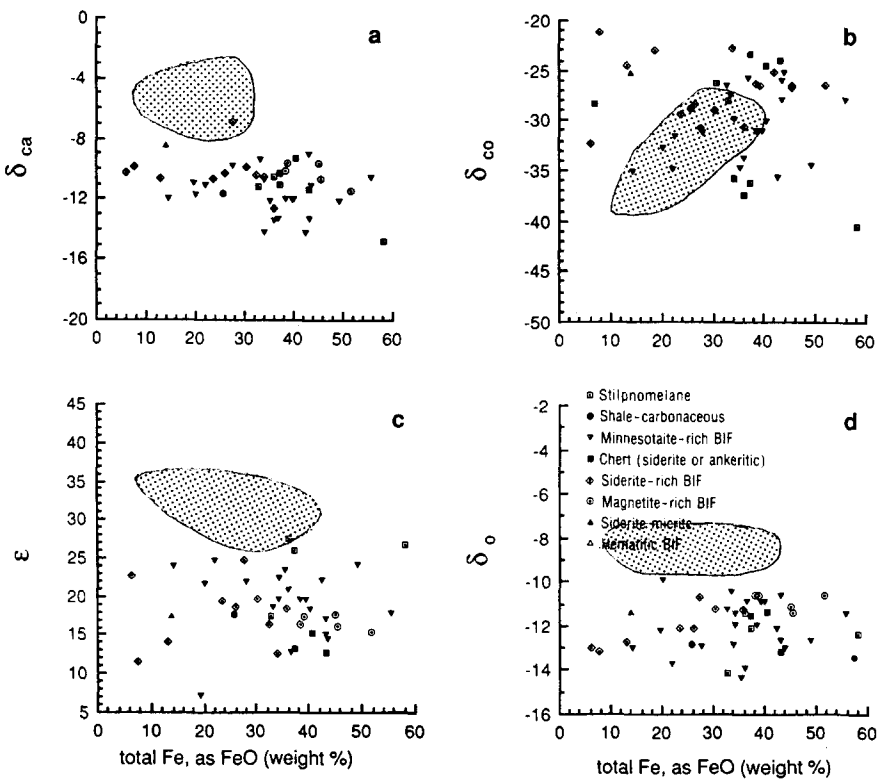

Fig. 9. Crossplots of abundance of total Fe (as FeO) vs. δ_o vs. δ_{ca}, δ_{co}, and ϵ in whole-rock samples from various lithofacies in the zone of contact metamorphism within the Groenwater Member of the Kuruman Iron Formation. Stippled region represents the range of Fe abundance and isotopic composition of siderite-rich BIF samples from similar lithofacies in the underlying Campbellrand–Kuruman transition zone.

between successive chert and siderite microbands.

In comparison with samples of similar lithology from the underlying Campbellrand–Kuruman transition zone, carbonate samples from within the metamorphic aureole are depleted in ^{13}C and ^{18}O. The abundance and C-isotopic composition of TOC in whole-rock samples are lower and more enriched than those in samples outside of the metamorphic aureole.

Although large variations in BIF lithologies make direct comparisons difficult, isotopic systematics in BIF sediments altered by contact metamorphism are similar to those noted in siliceous dolomites and limestones altered by similar thermal processes. The most distinct isotopic and elemental trends occur within 10 m of the diabase sill suggesting that volatilization and fluid infiltration associated with the intrusion were the main processes of alteration. Further studies on the O isotope compositions of cherts and carbonates in the zone of intense contact metamorphism may help to elucidate fluid/rock ratios, variations in the permeability of different lithofacies, as well as the temperature gradient extending from diabase sill into the BIF sediments

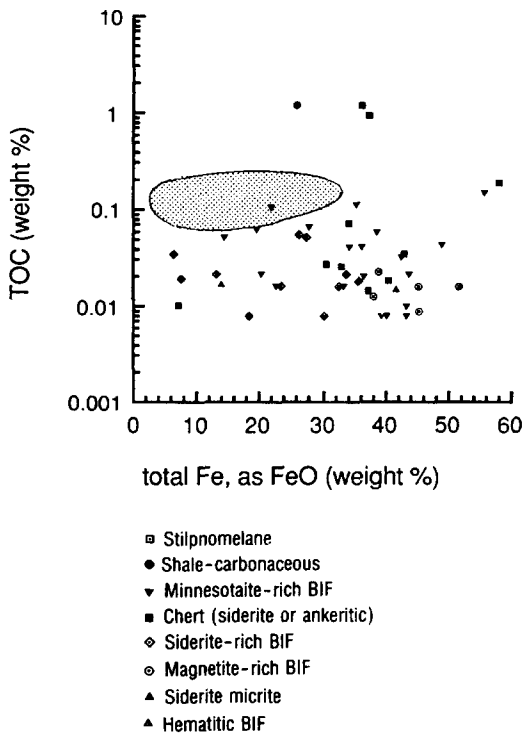

Fig. 10. Crossplot of abundance of total Fe (as FeO) vs. abundance of TOC in whole-rock samples from various lithofacies in the zone of contact metamorphism within the Groenwater Member of the Kuruman Iron Formation. Stippled region represents the range of Fe and TOC abundances in siderite-rich BIF samples from similar lithofacies in the underlying Campbellrand–Kuruman transition zone.

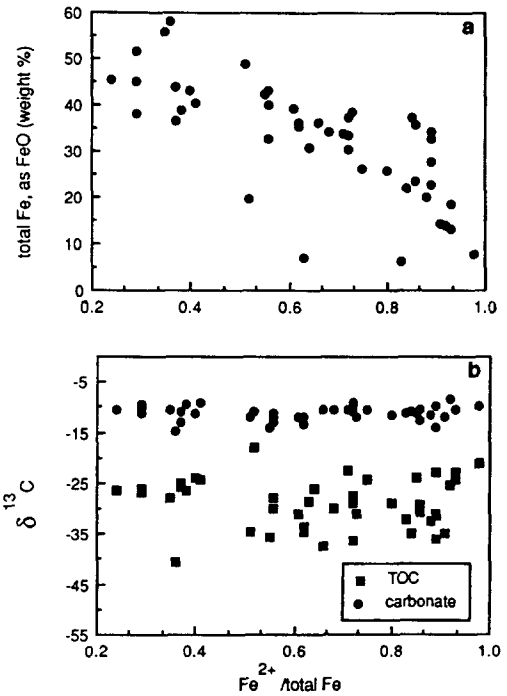

Fig. 11. Crossplot of (a) total Fe and (b) isotopic composition of carbonate (δ_{ca}) and TOC (δ_{co}) vs. oxidation state of Fe (as Fe^{2+}/total Fe) in whole-rock samples from various lithofacies in the zone of contact metamorphism within the Groenwater Member of the Kuruman Iron Formation

Acknowledgements

Materials for this study were generously made available to N. Beukes and C. Klein by the geological staff of the Griqualand Exploration and Finance Company (GEFCO), Kuruman, South Africa. I wish to thank the Department of Earth and Planetary Sciences at Harvard University for funds to travel to South Africa in the summer of 1990, and to my hosts N.J. Beukes and B. Cairncross at Rand Africaans University. Isotopic analyses of carbonates and cherts

were prepared and analyzed during the course of my dissertation at Indiana University in the laboratories of J.M. Hayes and E.M. Ripley. Many thanks go to S. Studley for assistance in the mass spectrometer facility, and J.M. Hayes, C. Klein, E.M. Ripley, A.H. Knoll, and H.D. Holland for their comments and criticisms on earlier versions of this paper. In addition, I wish to thank P. Mozley and J. Karhu for their thorough reviews and suggestions. This work was supported in part by NASA grant NGR 15-003-118 to J.M. Hayes and NSF grant EAR 84-19161 to C. Klein.

References

Baur, M.E., Hayes, J.M., Studley, S.A. and Walter, M.R., 1985. Millimeter-scale variations of stable isotope abundances in carbonates from banded iron-formations in the Hamersley Group of Western Australia. Econ. Geol., 80: 270–282.

Becker, R.H. and Clayton, R.N., 1976. Oxygen isotope study of a Precambrian banded iron-formation, Hamersley Range, Western Australia. Geochim. Cosmochim. Acta, 40: 1153–1165.

Beukes, N.J., 1980. Suggestions towards a classification and nomenclature for iron-formation. Trans. Geol. Soc. S. Afr., 83: 285–290.

Beukes, N.J., 1983. Palaeoenvironmental setting of iron-formation in the depositional basin of the Transvaal Supergroup, South Africa. In: A.F. Trendall and R.C. Morris (Editors), Iron-Formations: Facts and Problems. Elsevier, Amsterdam, pp. 131–209.

Beukes, N.J., 1984. Sedimentology of the Kuruman and Griquatown Iron Formations, Transvaal Supergroup, Griqualand West, South Africa. Precambrian Res., 245: 47–84.

Beukes, N.J., 1987. Facies relations, depositional environments and diagenesis in a major early Proterozoic stromatolitic carbonate platform to basinal sequence, Campbellrand Subgroup, Transvaal Supergroup, southern Africa. Sediment. Geol., 54: 1–46.

Beukes, N.J., Klein, C., Kaufman, A.J. and Hayes, J.M., 1990. Carbonate petrography, kerogen distribution and carbon and oxygen isotope variations in an Early Proterozoic transition from limestone to iron-formation deposition, Transvaal Supergroup, South Africa. Econ. Geol., 85: 663–690.

French, B.M., 1971. Stability relations of siderite ($FeCO_3$) in the system Fe–C–O. Am. J. Sci., 271: 37–78.

French, B.M., 1973. Mineral assemblages in diagenetic and low-grade metamorphic iron formations. Econ. Geol., 68: 1063–1075.

Gole, M.J., 1980. Mineralogy and petrology of very-low metamorphic grade Archean banded iron-formations, Weld Range, Western Australia. Am. Mineral., 65: 8–25.

Gregory, R.T. and Criss, R.E., 1986. Isotopic exchange in open and closed systems. In: J.W. Valley, H.P. Taylor and J.R. O'Neil (Editors), Stable Isotopes in High Temperature Geological Processes. Mineral. Soc. Am. Rev. Mineral., 16: 91–127.

Haase, C.S., 1982. Metamorphic petrology of the Negaunee Iron Formation, Marquette district, northern Michigan: mineralogy, metamorphic reactions and phase equilibria. Econ. Geol., 77: 60–81.

Holland, H.D. and Beukes, N.J., 1990. A paleoweathering profile from Griqualand West, South Africa: evidence for a dramatic rise in atmospheric oxygen between 2.2 and 1.9 bybp. Am. J. Sci., 290-A: 1–34.

Kaufman, A.J., Hayes, J.M. and Klein, C., 1990. Primary and diagenetic controls of isotopic compositions of iron-formation carbonates. Geochim. Cosmochim. Acta, 54: 3461–3473.

Klein, C., 1974. Greenalite, stilpnomelane, minnesotaite, crocidolite and carbonates in a very low-grade metamorphic Precambrian iron-formation. Can. Mineral., 12: 475–498.

Klein, C. and Beukes, N.J., 1989. Geochemistry and sedimentology of a facies transition from limestone to iron-formation deposition in the early Proterozoic Transvaal Supergroup, South Africa. Econ. Geol., 84: 1733–1774.

Klein, C. and Bricker, O.P., 1977. Some aspects of the sedimentary and diagenetic environment of Proterozoic banded iron-formation. Econ. Geol., 72: 1457–1470.

LaBerge, G.L., 1966. Altered pyroclastic rocks in South African iron-formation. Econ. Geol, 61: 572–581.

Miyano, T., 1987. Diagenetic to low-grade metamorphic conditions of Precambrian iron-formations. In: P.W.U. Appel and G.L. LaBerge (Editors), Precambrian Iron-Formations. Theophrastus Publications, Athens, pp. 155–186.

Miyano, T. and Beukes, N.J., 1984. Phase relations of stilpnomelane, ferriannite and riebeckite in very low-grade metamorphosed iron-formations. Trans. Geol. Soc. S. Afr., 87: 111–124.

Miyano, T. and Klein, C., 1986. Fluid behavior and phase relations in the system Fe–Mg–Si–C–O–H: application to high-grade metamorphism of iron-formation. Am. J. Sci., 286: 540–575.

Miyano, T. and Klein, C., 1989. Phase equilibria in the system K_2O–FeO–MgO–Al_2O3–SiO_2–H_2O–CO_2 and the stability limit of stilpnomelane in metamorphosed Precambrian iron-formations. Contrib. Mineral. Petrol., 102: 478–491.

Perry, E.C. and Ahmad, S.N., 1983. Oxygen isotope geochemistry of Proterozoic chemical sediments. In: L.D. Mendaris Jr., C.W. Byers, D.M. Mickelson and W.C. Shanks (Editors), Proterozoic Geology: Selected Papers from an International Proterozoic Symposium. Geol. Soc. Am. Mem., 161: 253–263.

Perry, E.C., Tan, F.C. and Morey, G.B., 1973. Geology and stable isotope geochemistry of the Biwabik Iron Formation, Northern Minnesota. Econ. Geol., 68: 1110–1125.

Robie, R.A., Haselton, H.T., Jr. and Hemingway, B.S., 1984. Heat capacities and entropies of rhodochrosite ($MnCO_3$) and siderite ($FeCO_3$) between 5 and 600 K. Am. Mineral., 69: 349–357.

Sumner, D.Y. and Bowring, S.A., 1996. U–Pb geochronologic constraints on deposition of the Campbellrand Subgroup, Transvaal Supergroup, South Africa. In: A. Danielson and A.J. Kaufman (Editors), Geology and Geochemistry of the Transvaal Supergroup. Precambrian Res., 79: 25–35 (this issue).

Trendall, A.F. and Blockley, J.G., 1970. The iron formations of the Precambrian Hamersley Group, Western Australia, with special reference to the associated crocidolite. Geol. Surv. W. Aust., Bull., 119, 366 pp.

Valley, J.W., 1986. Stable isotope geochemistry of metamorphic rocks. In: J.W. Valley, H.P. Taylor and J.R. O'Neil (Editors), Stable Isotopes in High Temperature Geological Processes. Mineral. Soc. Am. Rev. Mineral., 16: 445–486.

Valley, J.W. and O'Neil, J.R., 1981. $^{13}C/^{12}C$ exchange between calcite and graphite: a possible thermometer in Grenville marbles. Geochim. Cosmochim. Acta, 45: 411–419.

Winter, B.L. and Knauth, L.P., 1992. Stable isotope geochemistry of cherts and carbonates from the 2.0 Ga Gunflint Iron Formation: implications for the depositional setting, and the effects of diagenesis and metamorphism. Precambrian Res., 59: 283–313.